Advanced Ceramics Progress: Vol. 10, No. 2, (Spring 2024) 40-46

Materials and Energy Research Center
MERC

Contents lists available at ACERP

Advanced Ceramics Progress

Journal Homepage: www.acerp.ir

Original Research Article

The Influence of Diameter and Morphology on Magnetic Properties of Strontium Ferrite Nanofibers

Mahdieh Akbari Gandomani [a], Ali Ghasemi [b], Shahab Torkian [c], Zahra Rahmani Boldaji [a]*

[a] *Master, Department of Materials Engineering, Malek Ashtar University of Technology, Shahin shahr, Isfahan, Iran.*
[b] *Professor, Department of Materials Engineering, Malek Ashtar University of Technology, Shahin shahr, Isfahan, Iran.*
[c] *Assistant Professor, Department of Materials Engineering, Malek Ashtar University of Technology, Shahin shahr, Isfahan, Iran.*

* Corresponding Author Email: zah.ra.hmani111@gmail.com (Zahra. Rahmani Boldaji) URL: https://www.acerp.ir/article_212296.html

ARTICLE INFO

Article History:
Received: 01 November 2024
Revised: 23 November 2024
Accepted: 29 December 2024

Keywords:
Ceramic Nanofibers
$SrFe_{12}O_{19}$
Electrospinning
Magnetic Ceramics
Nanomaterials

ABSTRACT

Due to the wide range of applications of strontium ferrite in various industries and the increasing demand for lightweight devices with enhanced magnetic properties, this study aims to fabricate and optimize the magnetic performance of strontium ferrite nanofibers using the electrospinning method. The purpose of this research is to investigate the effects of different polyvinylpyrrolidone (PVP) concentrations and electrospinning parameters—such as applied voltage, feed rate, and the distance between the collector and nozzle—on the microstructure and magnetic properties of the nanofibers. The results of energy-dispersive spectroscopy (EDS) confirmed the presence of Fe, O, and Sr elements, while X-ray diffraction (XRD) analysis indicated the successful synthesis of single-phase strontium ferrite. Field-emission scanning electron microscopy (FE-SEM) images showed that optimizing the electrospinning parameters resulted in nanofibers with diameters of less than 100 nm and considerable lengths. Vibrating sample magnetometry (VSM) analysis of the optimized sample yielded a saturation magnetization of 60 $A \cdot m^2/kg$, residual magnetization of 23 $A \cdot m^2/kg$, and a coercivity of 4.29×10^5 A/m. The high coercivity is attributed to shape anisotropy in the nanofibers. These results demonstrate that, by carefully adjusting electrospinning parameters, strontium ferrite nanofibers with desirable magnetic properties can be successfully fabricated.

https://doi.org/10.30501/acp.2024.486473.1168

1. INTRODUCTION

Magnetic ferrites are essential ceramic materials widely used in industry and technology. Among the various ferrites, M-type ferrites, including strontium ferrite, are considered hard magnetic materials with a hexagonal magnetoplumbite structure (Pullar et al., 2012). Strontium ferrite, with the molecular formula $SrFe_{12}O_{19}$, exhibits excellent magnetic properties such as high saturation magnetization, excellent coercivity, a large anisotropy constant along the c-axis, a high Curie temperature, desirable chemical stability, and high corrosion resistance. These properties make it a promising material for future applications (Lu et al., 2011; Shen et al., 2010). Strontium ferrite is used in electromagnetic wave absorption, permanent magnets, microwave-generating devices, high-density magnetic memories, sound recording devices, small electric motors, telecommunications and electronics industries, and sensors (Jing et al., 2015; Gupta et al., 2024; Liu et al., 2015). However, the bulk form of strontium ferrite presents limitations, such as high weight, which restricts its application in adsorbent technologies. As a result, reducing the material's weight while maintaining its beneficial properties has become a critical challenge in

Please cite this article as: Akbari Gandomani, M., Ghasemi, A., Torkian, Sh. & Rahmani Boldaji, Z. (2024). The Influence of Diameter and Morphology on Magnetic Properties of Strontium Ferrite Nanofibers, *Advanced Ceramics Progress*, 10(2), 40-46. https://doi.org/10.30501/acp.2024.486473.1168

extending its potential applications (Shen et al., 2012). Various morphologies, including nanoparticles, thin layers, and nanofibers, have been explored to overcome this limitation, utilizing techniques such as drawing (Ramakrishna et al., 2005), solvothermal synthesis, precursor thermal decomposition (Wang et al., 2002), laser ablation (Morales et al., 1998), and electrospinning. Among these, the electrospinning technique stands out as a versatile method for producing one-dimensional nanostructures, such as nanotubes, nanofibers, and nanoribbons. It enables the fabrication of fibers with diameters ranging from micrometers to nanometers and has garnered significant attention due to its simplicity and widespread use (Yang et al., 2014). The resulting nanofibers exhibit unique properties, including a high specific surface area and a high aspect ratio (Dabirian et al., 2010). Moreover, in magnetic nanofibers, shape anisotropy plays a more significant role than in nanoparticles and bulk samples, which further enhances their magnetic performance (Mathews et al., 2021). Although significant research has been conducted on fabricating strontium ferrite nanofibers, many studies have focused on optimizing the processing conditions and analyzing the influence of temperature on morphology and magnetic properties. For instance, in 2009, Shen et al. prepared composite fibers of $SrFe_{12}O_{19}$/polyvinylpyrrolidone using sol-gel-assisted electrospinning, revealing the critical role of calcination temperature in determining fiber characteristics (Cong-ju et al., 2011). However, more detailed investigations are needed to enhance the magnetic properties of strontium ferrite nanofibers by optimizing electrospinning parameters. This study addresses this gap by synthesizing strontium ferrite nanofibers through electrospinning, with careful control of the solution preparation and key electrospinning parameters, such as applied voltage, nozzle-to-collector distance, and flow rate. Microstructural analyses were performed using X-ray diffraction (XRD) and field emission scanning electron microscopy (FE-SEM) to characterize the morphology and diameter of the nanofibers. Additionally, the magnetic properties were evaluated using a vibrating sample magnetometer (VSM).

2. MATERIALS AND METHODS

1.2. Materials

Strontium (II) nitrate hexahydrate (99%, Merck Co.) and iron (III) nitrate nonahydrate (99%, Merck Co.) were used as the metal precursors. Citric acid anhydrous ($C_6H_8O_7 \cdot H_2O$, 99%, Merck Co.) was also employed as a chelating agent. Polyvinylpyrrolidone (PVP, M_w = 500,000, Merck Co.) was utilized as a polymer-based matrix. N, N-dimethylformamide (DMF, 99.5%, Merck Co.), ethanol (C_2H_5OH, 99.5%, Merck Co.), and deionized water were used as solvents.

2.2. Synthesis

Strontium ferrite nanofibers were synthesized through a multi-step process, beginning with the preparation of an electrospinning solution using the sol-gel method. A polymer solution was first prepared by dissolving varying amounts of polyvinylpyrrolidone (PVP) in a mixture of 7 ml deionized water and 13 ml ethanol, resulting in a polymer solution of different concentrations. The water content in the solution is a critical factor that influences the hydrolysis rate of the metal precursors during the sol-gel process. Hydrolysis, the reaction between water and metal precursors, plays a key role in forming metal hydroxides that transition into the oxide phase. Water acts as a catalyst in this reaction, and its amount affects the hydrolysis rate. Higher water content generally speeds up hydrolysis, leading to the formation of hydroxyl groups and early gelation. However, excessive water may result in incomplete gelation or the formation of undesirable phases that negatively impact the material properties.

The ferrite solution was then prepared by dissolving 0.2 g of strontium nitrate hexahydrate, 4.6 g of iron nitrate nonahydrate, and a specified amount of citric acid as a chelating agent in a mixture of 10 ml dimethylformamide (DMF) and 5 ml deionized water. The solution was stirred for 20 hours to ensure thorough mixing. The presence of water is essential for hydrolyzing the metal salts, facilitating the formation of a stable gel. The hydrolysis rate, influenced by the water content, determines how quickly the ferrite network forms, affecting the final structural and magnetic properties of the nanofibers (Huang et al., 2024; Kim et al., 2024). The resulting ferrite solution was loaded into a plastic syringe with a stainless-steel needle, which was fixed to a digitally controlled syringe pump as part of the electrospinning apparatus. Electrospinning was performed by applying varying voltages, flow rates, and distances between the nozzle tip and an aluminum collector drum. Different concentrations of PVP and electrospinning parameters were used to produce the nanofiber samples.

After electrospinning, the obtained nanofiber mats were dried in air at 200 °C for 5 hours. The dried mats were then calcined in air at 800 °C with a heating rate of 3 °C/min for 3 hours to ensure complete crystallization of the strontium ferrite phase.

3.2. Characterization

The synthesized nanofibers were analyzed by X-ray diffraction using an X'Pert Pro X-ray diffractometer (ASENWARE) with Cu Kα radiation (λ = 0.154 nm) at a generator voltage of 40 kV. The morphology of the electrospun nanofibers was investigated by field emission scanning electron microscopy (FE-SEM: MIRA3 TESCAN). The magnetic properties of the $SrFe_{12}O_{19}$ nanofibers were measured at room temperature using a vibrating sample magnetometer (VSM;

Meghnatis Daghigh Kavir Co., Iran) with a maximum applied field of 8 ×10^5 A/m.

3. RESULTS AND DISCUSSION

1.3. Structural Investigation

Figure 1 shows the X-ray diffraction pattern of strontium ferrite nanofibers with different concentrations of polymer after calcination at 800 °C for 3 hours. As shown in the figure, the high intensity of the peaks related to the (110), (017), and (114) planes indicates the formation of strontium ferrite nanofibers with a magnetoplumbite structure, free from impurities. The lattice parameter and crystallite size, obtained using the Scherrer equation, are reported in Table 1.

$$\beta = \frac{K\lambda}{L\cos\theta} \quad (1)$$

where β is the full width at half maximum (FWHM) of the diffraction peak, λ the X-ray wavelength in nanometers (nm), L the crystallite size, and K a constant related to crystallite shape, typically taken as 0.9.

$$a = \frac{n\lambda}{2\sin\theta}\sqrt{h^2 + k^2 + l^2} \quad (2)$$

where n is the order of reflection (usually n=1 for the first order), λ the wavelength of the X-ray, d the interplanar spacing, and θ the Bragg angle.

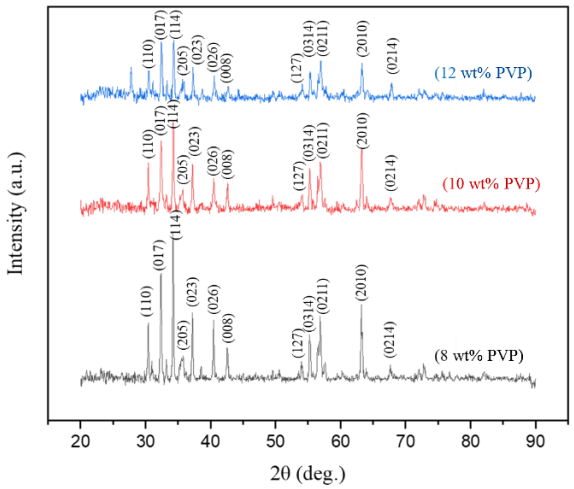

Figure 1. XRD patterns of the $SrFe_{12}O_{19}$ nanofibers with different concentrations of PVP, calcined at 800 °C for 3 hours

TABLE 1. Crystallite size (L) and lattice parameter of the randomly oriented nanofibers with different concentrations of PVP

wt% PVP	a (Å)	c (Å)	c/a	V (Å^3)	L (Å)
8	5.23	20.87	3.99	494.93	593
10	5.23	20.87	3.99	494.93	639
12	5.22	20.88	4	493.04	361

2.3. Morphological Study

FE-SEM images of electrospun $SrFe_{12}O_{19}$ nanofibers are shown in Figures 2 and 3. Data obtained from the images indicate that the average diameter of the fibers is less than 100 nm. Figure 2, which pertains to $SrFe_{12}O_{19}$ nanofibers with PVP concentrations of 8 wt% and 12 wt%, shows that the diameter of the nanofibers increased from 65 nm to 73 nm with increasing polymer concentration. Higher polymer concentration increases the viscosity of the electrospinning solution. Increased viscosity results in greater chain entanglement within the solution, which helps form more stable and thicker jets during electrospinning, leading to larger fiber diameters

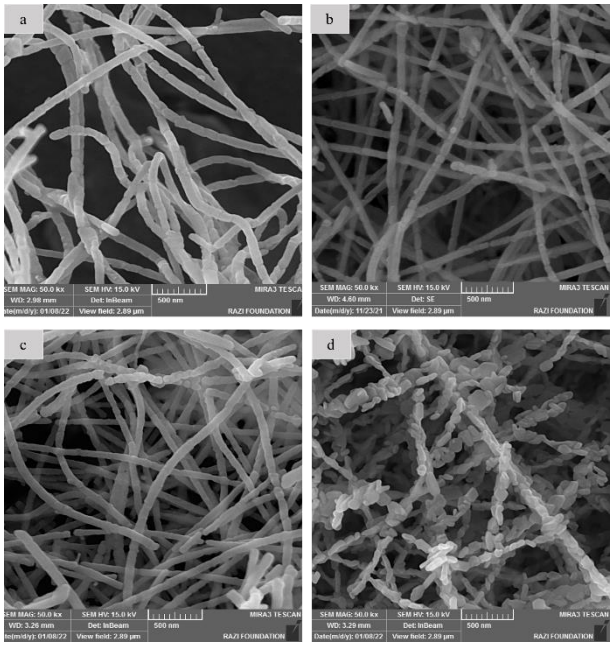

Figure 2. FE-SEM images of $SrFe_{12}O_{19}$ nanofibers obtained at nozzle tip to collector distance of 19 cm, flow rate of 1 ml/h, 15 kV voltage, and various concentration of polymer: (a) 8 wt% PVP, (b) 12 wt% PVP

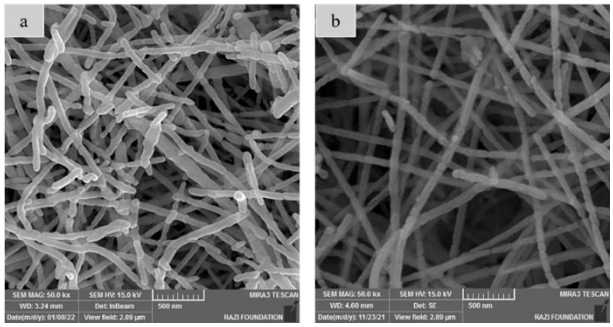

Figure 3. FE-SEM images of sintered $SrFe_{12}O_{19}$ nanofibers with 12 wt% PVP obtained at nozzle tip to collector distance of 19 cm, flow rate of 1 ml/h, and various voltages: (a) 13 kV, (b) 15 kV, (c) 18 kV, and (d) 21 kV

(Huang et al., 2003). Increased polymer concentration can also affect the solution's conductivity. Although this can sometimes lead to finer fibers, the dominant effect in many cases is that higher viscosity overrides the influence of conductivity, resulting in thicker fibers (Mituppatham et al., 2004) . Figure 3 shows $SrFe_{12}O_{19}$

nanofibers produced at different applied voltages during electrospinning: (a) 13 kV, (b) 15 kV, (c) 18 kV, and (d) 21 kV. As shown in Figure 3, with an increase in voltage from 13 kV to 18 kV, the diameter of the nanofibers decreases. With an increase in the applied voltage, the electrostatic force increases, resulting in greater stretching of the solution and a decrease in fiber diameter. At a voltage of 21 kV, bead structures are formed instead of fiber structures. This occurs because, at very high voltages, the stretching force becomes excessive, leading to jet instability and the formation of beads instead of continuous fibers (Deitzel et al. 2001).

3.3. Magnetic Properties

The magnetic properties of the $SrFe_{12}O_{19}$ nanofibers were measured using VSM at room temperature. The pertinent details of coercivity (H_c), saturation magnetization (Ms), and remanent magnetization (Mr) are shown in Table 2. The results demonstrate good single-phase magnetic behavior, with all hysteresis loops exhibiting hard magnetic characteristics. Figure 4(a) shows the hysteresis loops of the nanofibers obtained at two applied voltages during electrospinning, 15 kV and 18 kV. With increasing applied voltage and decreasing nanofiber diameter, the coercivity increases from 3.84×10^5 A/m to 4.10×10^5 A/m according to Equation (3).

$$H_c \approx \frac{K}{\mu_0 M_s}\left(\frac{L}{D}\right) \quad (3)$$

where K is the anisotropy constant, μ0 the permeability of free space, M_s the saturation magnetization, L the characteristic length over which domain walls move, and D the particle diameter (Supekar et al., 2024).

Figure 4(b) shows the hysteresis loops of strontium ferrite nanofibers produced at different feed rates. The coercivity (Hc) consistently decreases from 3.90×10^5 A/m to 3.83×10^5 A/m as the feed rate increases from 0.5 ml/h to 1.5 ml/h. This decrease in Hc can also be explained by Equation (3). The diameter of the nanofibers increases with an increasing flow rate because the jet takes longer to dry at higher flow rates (Na et al., 2018). Magnetic hysteresis loops of strontium ferrite nanofibers produced at different distances between the collector and nozzle tip are exhibited in Figure 4(c). The increase in coercivity from 7 cm to 15 cm indicates that, with increasing distance, the fibers have more time to solidify and form a more uniform structure. This reduces surface defects and allows for a more consistent magnetic domain structure, increasing coercivity (Y et al., 2004). This trend aligns with the understanding that better-formed nanofibers with fewer defects and more uniform sizes have higher coercivity due to more stable magnetic domains (Pillay et al., 2013).

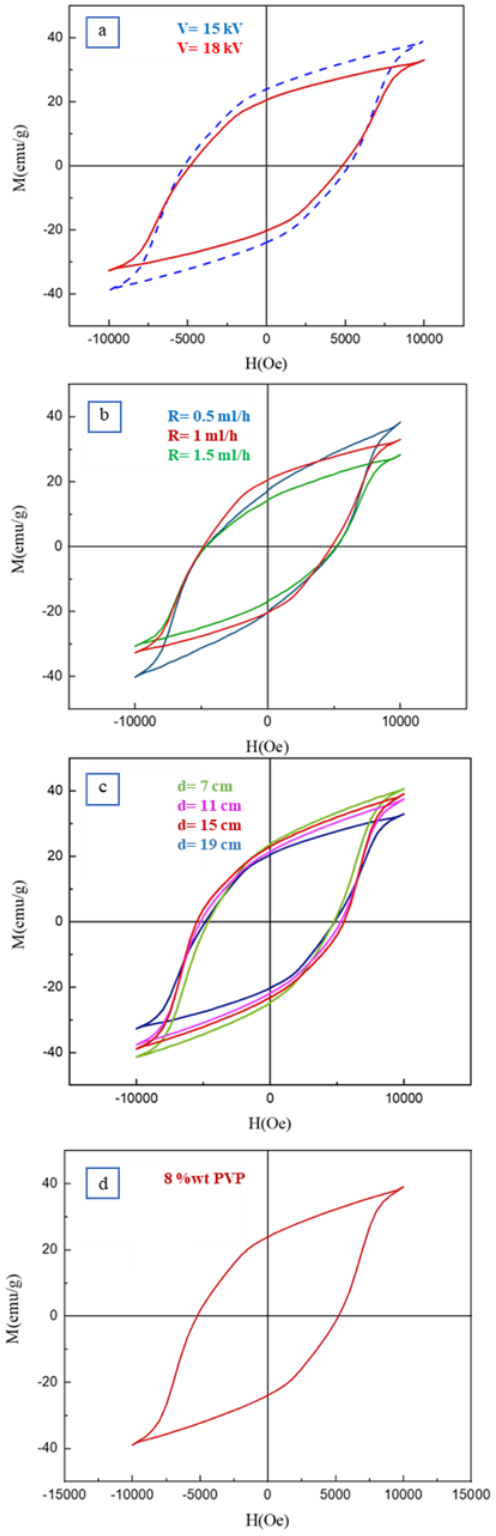

Figure 4. (a) Hysteresis loops of the randomly oriented $SrFe_{12}O_{19}$ nanofibers obtained at 15 kV and 18 kV applied voltages. (b) Hysteresis loops of nanofibers obtained at 0.5 ml/h, 1 ml/h and 1.5 ml/h flow rates. (c) Hysteresis loops of nanofibers obtained at different distances between nozzle tip and collector. (d) Hysteresis loop of nanofibers with 8 wt% PVP

The decrease in coercivity at 19 cm suggests that, at this longer distance, the benefits of increased evaporation time are outweighed by other factors such as jet instability or over-evaporation. This could lead to fibers with more surface defects or inconsistent diameters, reducing coercivity (Teo et al., 2006).

This result highlights the importance of balancing the distance to optimize fiber uniformity and magnetic properties (Sill et al., 2008). Figure 4(d) shows the hysteresis loops of the strontium ferrite nanofibers obtained at polymer concentrations of 8 wt%. As shown in Table 2, with increasing amounts of PVP, the fiber diameter increases, causing the Hc to decrease from 4.20 × 10^5 A/m to 3.84 × 10^5 A/m according to Equation (3). Since the nanofibers are not fully saturated in the VSM analysis, the Law of Approach to Saturation (LAS), as shown in Equation (4), was used for an accurate determination of the saturation magnetization. The magnetic properties of all samples are reported in table 2.

$$M(H) = M_s\left(1 - \frac{a}{H} - \frac{b}{H^2}\right) + \aleph H \quad (4)$$

where M(H) presents the magnetization at a given applied magnetic field (H), M_s stands for the saturation magnetization, and a and b are fitting parameters that account for deviations from saturation. The terms $\frac{a}{H}$ and $\frac{b}{H^2}$ represent the approach to saturation. As H increases, these terms decrease, causing the magnetization to approach M_s. The term ℵH accounts for the linear increase in magnetization with the applied field due to the linear response of some magnetic moments not aligned with the applied field (Chitra Devi et al., 2019).

TABLE 2. magnetic properties of the randomly oriented $SrFe_{12}O_{19}$ nanofibers

Sample	$M_{s\,(VSM)}$ (A.m²/kg) & (emu/g)	$M_{s(LAS)}$ (A.m²/kg) & (emu/g)	M_r (A.m²/kg) & (emu/g)	H_c (A/m) (Oe)
8 wt% PVP	47	68	28	4.20 × 10^5 5281
12 wt% PVP	33	54	20	3.84 × 10^5 4828
Voltage of 15 kV	33	54	20	3.84 × 10^5 4828
Voltage of 18 kV	39	62	24	4.10 × 10^5 5153
Flow rate of 0.5 ml/h	38	65	19	3.90 × 10^5 4899
Flow rate of 1.0 ml/h	33	54	20	3.84 × 10^5 4828
Flow rate of 1.5 ml/h	28	46	16	3.83 × 10^5 4814
Distance of 7 cm	41	63	33	3.70 × 10^5 4643
Distance of 11 cm	38	62	22	4.12 × 10^5 5184
Distance of 15 cm	39	60	23	4.29 × 10^5 5390
Distance of 19 cm	33	54	20	3.84 × 10^5 4828

4. CONCLUSION(S)

In this study, electrospinning was utilized to fabricate strontium ferrite nanofibers, which were subsequently calcined at 800°C. X-ray diffraction (XRD) confirmed the formation of a single-phase structure. Investigations into the magnetic and structural properties using FE-SEM, XRD, and VSM revealed significant outcomes. Higher polymer concentrations in the electrospinning solution were correlated with larger nanofiber diameters, with notable effects on coercivity observed in samples containing PVP concentrations of 8 wt% and 12 wt%. The optimized sample, processed at 800°C with 12 wt% PVP, exhibited excellent magnetic properties, achieving a coercivity of 4.29×10^5A/m and a saturation magnetization of 60.05 A·m²/kg. Additionally, increasing the electrospinning voltage effectively reduced nanofiber diameters. This was evident in SEM images, where distinctive bead-like structures appeared at 21 kV. These findings underscore the potential of electrospinning for precisely tailoring the magnetic and structural characteristics of strontium ferrite nanofibers, presenting promising possibilities for applications in advanced magnetic materials.

ACKNOWLEDGEMENTS

We gratefully acknowledge Department of Materials Engineering, Malek Ashtar University of Technology, Isfahan, Iran for financial support.

NOMENCLATURE

a and b in Equation (4)	Fitting parameters in LAS equation
a and c in Table (1)	Lattice parameters for unit cell dimensions
d	Interplanar spacing
D	Fiber diameter impacting magnetic properties
DMF	N, N-dimethylformamide, a solvent
EDS	Energy-dispersive X-ray spectroscopy
FE-SEM	Field emission scanning electron microscopy diameter
H_c	Field strength needed to demagnetize
K	Anisotropy constant
L	Average crystal size
LAS	Method for determining saturation magnetization, particularly when full saturation isn't reached in VSM's range
M(H)	Magnetization at a given field
Miller Indices	Crystal planes orientation notation
M_r	Magnetization left after the field is removed
M_s	Maximum magnetization achievable
M_s (LAS)	Saturation magnetization using LAS method
PVP	Polyvinylpyrrolidone, a polymer-based matrix
$SrFe_{12}O_{19}$	Strontium ferrite
V	Unit cell volume
VSM	Vibrating sample magnetometer
XRD	X-ray diffraction
β	Full width at half maximum (FWHM) of the diffraction peak
λ	X-ray wavelength
μ_0	Magnetic field production constant
א	Accounts for linear magnetization increase in LAS

REFERENCES

1. Chitra Devi, E., & Soibam, I. (2019). Law of approach to saturation in Mn–Zn ferrite nanoparticles. *Journal of Superconductivity and Novel Magnetism*, *32*. https://doi.org/10.1007/s10948-018-4823-4
2. Cong-ju, L., & Xu, G. (2011). Template preparation of strontium hexaferrite ($SrFe_{12}O_{19}$) micro/nanostructures: Characterization, synthesis mechanism and magnetic properties. *Materials Research Bulletin*, *46*, 119-123. https://doi.org/10.1016/j.materresbull.2010.09.030
3. Dabirian, F., Hosseini Ravandi, S. A., & Pishevar, A. (2010). Investigation of parameters affecting PAN nanofiber production using electrical and centrifugal forces as a novel method. *Current Nanoscience*, *6*, 545-552. https://doi.org/10.2174/157341310797575078
4. Deitzel, J., Kleinmeyer, J., Harris, D. E. A., & Tan, N. B. (2001). The effect of processing variables on the morphology of electrospun nanofibers and textiles. *Polymer*, *42*, 261-272. https://doi.org/10.3390/nano10061077
5. Gupta, A., & Roy, P. K. (2024). Improved strontium hexaferrites: An overview of current progress in synthesis, properties, and applications. *Materials Science and Engineering: B*, *306*, 117458. https://doi.org/10.1016/j.mseb.2024.117458
6. Huang, Z.-M., Zhang, Y., & Kotaki, M. (2003). A review on polymer nanofibers by electrospinning and their applications in nanocomposites. *Composites Science and Technology*, *63*, 2223-2253. https://doi.org/10.1016/S0266-3538(03)00178-7
7. Huang, X., Chen, K., Zhang, Z., Li, C., Li, P., Wang, X., & Lu, J. (2024). Study on the hydrolysis characteristics of polymeric aluminum chloride forced by fine bubbles and its key factors affecting the efficiency and capacity of forcing hydrolysis. *Water Research*, *250*, 122757. https://doi.org/10.1016/j.watres.2024.122757
8. Jing, P., Wang, Y., Wu, W., Li, H., & Yang, S. (2015). Width-controlled M-type hexagonal strontium ferrite ($SrFe_{12}O_{19}$) nanoribbons with high saturation magnetization and superior coercivity synthesized by electrospinning. *Scientific Reports*, *5*, 15089. https://doi.org/10.1038/srep15089
9. Kim, G., Kim, S., Jeong, H., & Chung, J. (2024). Numerical analysis of mixing performance in Y-junction mixers and its impact on yields from supercritical water hydrolysis. *The Journal of Supercritical Fluids*, *215*, 106425. https://doi.org/10.1016/j.supflu.2024.106425
10. Liu, G. F., Wang, S., Zhang, Y., & Xu, L. (2015). Magnetic properties and unusual morphologies of barium ferrites prepared by electrospinning and sol-gel auto-combustion method. *Materials Science Forum*, *815*, 141-146. https://doi.org/10.4028/www.scientific.net/MSF.815.141
11. Lu, Y., Yang, X. C., Zhu, J. L., Song, F. Z., & Shen, X. Q. (2011). Morphological and magnetic characteristics of strontium ferrite micro- and nanofibers. *Advanced Materials Research*, *399-401*, 736-740. https://doi.org/10.4028/www.scientific.net/AMR.399-401.736
12. Mathews, S., & Babu, D. (2021). Analysis of the role of M-type hexaferrite-based materials in electromagnetic interference shielding. *Current Applied Physics*, *29*. https://doi.org/10.1016/j.cap.2021.06.001
13. Mit-uppatham, C., Nithitanakul, M., & Supaphol, P. (2004). Ultrafine electrospun polyamide-6 fibers: Effect of solution conditions on morphology and average fiber diameter. *Macromolecular Chemistry and Physics*, *205*, 2327-2338. https://doi.org/10.1002/macp.200400225
14. Morales, A., & Lieber, C. (1998). A laser ablation method for the synthesis of crystalline semiconductor nanowires. *Science*, *279*, 208-211. https://doi.org/10.1126/science.279.5348.208
15. Na, K. H., Kim, J. H., & Kim, S. H. (2018). Fabrication and characterization of the magnetic ferrite nanofibers by electrospinning process. *Thin Solid Films*, *660*. https://doi.org/10.1016/j.tsf.2018.06.018
16. Pillay, V., de Jongh, J., & Choonara, Y. E. (2013). A review of the effect of processing variables on the fabrication of electrospun nanofibers for drug delivery applications. *Journal of Nanomaterials*, *2013*. https://doi.org/10.1155/2013/789289
17. Pullar, R. C. (2012). Hexagonal ferrites: A review of the synthesis, properties and applications of hexaferrite ceramics. *Progress in Materials Science*, *57(7)*, 1191–1334. https://doi.org/10.1016/j.pmatsci.2012.04.001
18. Ramakrishna, K. F. S., Teo, W.-E., Lim, T.-C., & Ma, Z. (2005). An introduction to electrospinning and nanofibers (p. 396). *World Scientific Publishing Co. Pte. Ltd*. https://doi.org/10.1142/9789812567611
19. Shen, X., Liu, M., Song, F., & Meng, X. (2010). Structural evolution and magnetic properties of $SrFe_{12}O_{19}$ nanofibers by electrospinning. *Journal of Sol-Gel Science and Technology*, *53(2)*, 448–453. https://doi.org/10.1007/s10971-009-2119-7
20. Shen, X., Yan, D., Wei, D., & Xu, Z. (2012). Shape anisotropy, exchange-coupling interaction and microwave absorption of hard/soft nanocomposite ferrite microfibers. *Journal of the American Ceramic Society*, *95(12)*, 3863-3870. https://doi.org/10.1111/j.1551-2916.2012.05375.x
21. Sill, T., & Recum, H. (2008). Electrospinning: Applications in drug delivery and tissue engineering. *Biomaterials*, *29*, 1989-2006. https://doi.org/10.1016/j.biomaterials.2008.01.011
22. Supekar, S., Gawde, M. S., & Bhagat, S. (2024). Relationship between structural and magnetic properties of 48Ni–52Fe laminates: Improvement study induced by annealing conditions. *Journal of Materials Science: Materials in Electronics*, *35*. https://doi.org/10.3390/nano10061077

23. Teo, W. (2006). A review on electrospinning design and nanofibre assemblies. *Nanotechnology*, *17*, R89-R106. https://doi.org/10.1088/0957-4484/17/14/R01

24. Wang, W., Liu, Y., Xu, C., Zheng, C., & Wang, G. (2002). Synthesis of NiO nanorods by a novel simple precursor thermal decomposition approach. *Chemical Physics Letters*, *362*, 119-122. https://doi.org/10.1016/S0009-2614(02)00996-X

25. Y, D., & Xia, Y. N. (2004). Electrospinning of nanofibers: Reinventing the wheel? *Advanced Materials*, *16*, 1151-1170. https://doi.org/10.1002/adma.200400719

26. Yang, Y., Liu, X., Jin, D., Huang, K., & Gao, S. (2014). The effects of the iron content on structural and magnetic properties of $Sr_{0.80}La_{0.20}Fe_xZn_{0.15}O_{19}$ hexagonal ferrites. *Journal of Magnetism and Magnetic Materials*, *355*, 254–258. https://doi.org/10.1016/j.jmmm.2013.12.010